ACS Photonics

Article

pubs.acs.org/journal/apchd5

Wavelength Scaling in Antenna-Enhanced Infrared Spectroscopy: Toward the Far-IR and THz Region

Ksenia Weber,[†] Maxim L. Nesterov,[†] Thomas Weiss,[†] Michael Scherer,[‡] Mario Hentschel,[†] Jochen Vogt,[§] Christian Huck,[§] Weiwu Li,[⊥] Martin Dressel,[⊥] Harald Giessen,[†] and Frank Neubrech*[,†]

[†]4th Physics Institute and Research Center SCoPE and [⊥]1. Physikalisches Institut and Research Center SCoPE, University of Stuttgart, Pfaffenwaldring 57, 70550 Stuttgart, Germany

[‡]InnovationLab GmbH and Institut für Hochfrequenztechnik, Technische Universität Braunschweig, Speyerer Straße 4, 69115 Heidelberg, Germany

[§]Kirchhoff Institute for Physics, Heidelberg University, Im Neuenheimer Feld 227, 69120 Heidelberg, Germany

Supporting Information

ABSTRACT: Weak vibrational signals in the infrared and terahertz spectral region can be enhanced by orders of magnitude when employing the electromagnetic near fields of plasmonic nanostructures. This approach is known as antenna-assisted surface-enhanced infrared absorption (SEIRA) and allows for a broad range of possible sensing applications. In the present work, we investigate the scaling of the SEIRA enhancement with wavelength, particularly toward the molecular fingerprint region (500−1500 cm^{-1}). We apply the concept of SEIRA to perform resonant antenna-enhanced spectroscopy of molecules in a spectral range from 4.5 to 45 THz (6.7−67 μm wavelength, 150−1500 cm^{-1}) using a standard Fourier transform infrared spectrometer. We fabricate arrays of rectangular gold antennas by electron-beam lithography and coat them with 30 nm thick layers of the fullerenes C_{60} and C_{70}, respectively. For the single digit THz measurements, we utilize spin-coated amino acids, particularly threonine. The resonances of the structures are tailored to spectrally match the molecular absorption features. An increased SEIRA enhancement of 2 orders of magnitude is found for antennas resonant at 6.7 THz when compared to 45 THz, corresponding to a λ^3 scaling over a frequency range of 1 order of magnitude. This scaling behavior is in excellent agreement with both numerical simulations and classical antenna theory. Further increase toward the single-digit THz region will yield the potential for ultrasensitive THz spectroscopy.

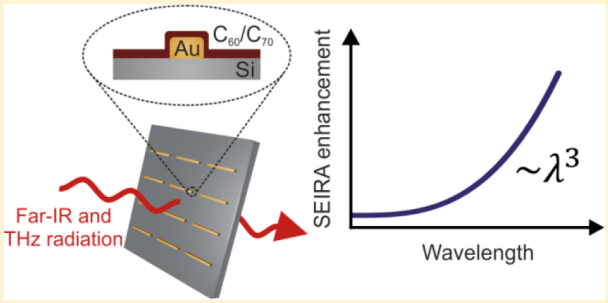

KEYWORDS: *surface-enhanced infrared absorption (SEIRA), plasmonic nanoantennas, IR spectroscopy, THz spectroscopy, molecular fingerprints, C_{60}, amino acids*

Terahertz spectroscopy is a label- and destruction-free technique for the identification and characterization of molecules based on their material-specific absorption features.[1] However, the low absorption cross section of these excitations limits its sensitivity to measurements of large numbers of molecules such as macroscopic pellets or solutions with high concentrations. Hence, improving the sensitivity of THz spectroscopy has been subject to research for many years, for example, by developing high power THz laser light sources.[2−6]

Another possibility to increase the sensitivity is the use of plasmonic structures, as has been demonstrated for other spectroscopic methods such as surface-enhanced fluorescence,[7,8] surface-enhanced Raman spectroscopy,[9,10] and surface-enhanced infrared absorption (SEIRA) spectroscopy[11−16] which allows for the detection of characteristic infrared (IR) molecular absorption features with high sensitivity by exploiting the strongly concentrated near fields around resonantly excited plasmonic structures. It was demonstrated that the vibrational absorption cross section of molecules is enhanced by up to 5 orders of magnitude if they are placed directly onto the nanoantenna.[17] Such resonant antenna-enhanced experiments are typically performed in the mid-infrared (MIR) regime, ranging from 37 to 100 THz (or 1250−3333 cm^{-1}, 3−8 μm wavelength, respectively).

In the THz spectral range the concept of coupling radiation to molecules via plasmonic structures is known from hybridization-induced transparency[18] and molecular sensing using single resonant nanoslits in thin metal layers.[19] In the latter method, small molecules are placed inside a THz nanoslit antenna, where their absorption cross section is strongly enhanced. The resulting change in the THz transmission of the nanoslit allows for ultrasensitive, but not material specific, molecular detection. In a different approach, the resonance shift of THz semiconductor plasmonic antennas was used to sense dielectric[20] and bacteria layers.[21] However, these experiments

Received: July 26, 2016
Published: December 12, 2016

DOI: 10.1021/acsphotonics.6b00534
ACS Photonics 2017, 4, 45−51

rely on THz time domain spectroscopy,[22,23] which intrinsically offers high incident field intensities, but is cost intensive and more complex than conventional Fourier transform infrared (FTIR) spectroscopy. Additionally, all of these techniques rely on simply monitoring a change of the plasmonic resonance and are not suited to obtain the spectroscopic fingerprint of the investigated material. This hampers the identification of unknown substances. In contrast to that, spectroscopic methods such as SEIRA enable the identification and characterization of unknown samples. Thus, it allows for the characterization of random samples and the acquisition of structural information.[24]

Following the approach of SEIRA, antenna-enhanced THz spectroscopy of semiconductor quantum dots was recently demonstrated.[25] The phonon resonance of a monolayer of cadmium selenide quantum dots located close to 6 THz could be detected. However, such optical phonon excitations offer substantially larger absorption cross sections than typical vibrational excitations of molecules.

On the one hand, performing such molecular spectroscopy at THz frequencies is especially challenging, as the wavelength of the THz radiation (300 μm at 1 THz) is huge compared to the dimensions of a molecule. On the other hand, the intensity of the plasmonic near fields in the vicinity of resonantly excited nanostructures is known to increase with structure size.[26−29] This increase in size corresponds to lower plasmonic resonance frequencies and can be understood in terms of an increased dipole moment and a smaller restoring force for larger antennas.[30] This near field scaling behavior suggests that performing SEIRA at frequencies toward the far-infrared and THz region might yield unprecedented sensitivities.

In the present work, we study the scaling behavior of the SEIRA enhancement of antennas resonant at frequencies toward the THz region. For this, we perform resonant antenna-enhanced spectroscopy of the organic molecules C_{60} and C_{70} using standard FTIR spectroscopy over a spectral range from 16 to 45 THz (6.7−18.7 μm wavelength, 533−1500 cm^{-1}). Both molecules exhibit characteristic vibrational absorption features in the molecular fingerprint region over a broad spectral range,[31] which are enhanced by resonantly tuned antennas. In addition, to access the single digit THz regime, we use the α-amino acid threonine to resonantly enhance and detect its vibrational absorption features in the spectral range from 4.5 to 10 THz (30−67 μm wavelength, 150−333 cm^{-1}). Our findings are compared to FDTD simulations of the plasmonic near fields of the antennas as well as to analytical calculations derived from classical antenna theory.

We fabricated gold antennas in periodic 200 × 200 μm^2 (for the investigation of C_{60} and C_{70}) and 1 × 1 mm^2 (for the investigation of the amino acid threonine) arrays (see Methods for details) on high resistivity float-zone silicon. A schematic of the array geometry can be seen in Figure 1a. Width w and thickness h of the nanoantennas were both fixed at $w = h = 100$ nm. The lateral spacing d_x was fixed at 1 μm for all arrays, while the transversal spacing d_y was varied to match the resonance position to the collective transversal excitation of the array, known as Rayleigh anomaly.[32,33] An additional enhancement of the near field intensity is known to take place when the fundamental antenna resonance is close to the collective excitation of the array.[34−37] To ensure a match of the plasmonic resonance with the investigated molecular absorption bands, arrays of varying antenna lengths were prepared. In the case of C_{60}, a transversal spacing of d_y = 1.6 μm and antenna lengths of

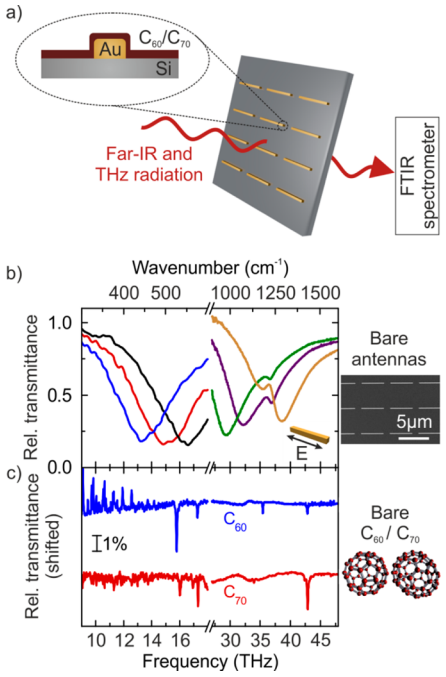

Figure 1. (a) Schematic drawing of investigated samples measured with an FTIR-spectrometer. (b) Relative transmittance (incident electric field parallel to the long antenna axis as indicated by the inset) of antennas of varying lengths [L = 4.4 (blue), 4.0 (red), 3.6 (black), 2.0 (green), 1.8 (purple), and 1.6 μm (yellow)]. The feature at 37.5 THz (1250 cm^{-1}) originates from the phonon excitation of the natural SiO_2 layer on top of the silicon substrate, see text. On the right, a scanning electron micrograph of an exemplary antenna array is shown. (c) Far- and mid-infrared transmittance of C_{60} and C_{70} films with a thickness of 30 nm. On the right, schematics of a C_{60} (left) and a C_{70} (right) molecule is shown with the carbon atoms represented as red spheres.

L = 1.1, 1.4, and 1.7 μm were chosen for the MIR region (here 900−1600 cm^{-1}), and a transversal spacing of d_y = 4.0 μm and antenna lengths of L = 3.2, 3.5, and 3.8 μm were chosen for the far-infrared (FIR; 400−650 cm^{-1}). In the case of C_{70} and the MIR spectral region, transversal spacing and antenna lengths were d_y = 1.9 μm and L = 1.2, 1.4, and 1.6 μm, while for the FIR d_y = 3.3 μm and L = 3.6, 3.8, and 4.0 μm were chosen. For the amino acid threonine and the single digit THz region (150−300 cm^{-1}) the geometric parameters were chosen as L = 6.9, 8.2, and 9.0 μm and d_y = 6.5, 7.5, and 8 μm, respectively.

To the right-hand side of Figure 1b, a scanning electron micrograph of an exemplary antenna array with an antenna length of L = 3.8 μm and a transversal spacing of d_y = 4.0 μm is shown.

RESULTS AND DISCUSSION

In Figure 1b, typical spectra of antenna arrays without molecular coating, measured with a resolution of 8 cm^{-1}, are plotted. The spectra were measured with light polarized along the long antenna axis. Reference measurements were performed on an unstructured part on the very same substrate. The absorption feature close to the plasmonic resonances located at 1250 cm^{-1} can be attributed to the excitation of a phonon-polariton of the natural silicon dioxide (SiO_2) layer on the substrate.[38]

After the deposition of the molecules, measurements were performed with a resolution of 1 cm^{-1} to resolve the narrow

DOI: 10.1021/acsphotonics.6b00534
ACS Photonics 2017, 4, 45−51

absorption bands. In perpendicular polarization to the antennas, no plasmonic resonances in the investigated spectral range and thus no enhanced near fields are excited. Note that, in the case of C_{60} and C_{70}, the background measurement is taken on the fullerene layer on the very same substrate. No molecular absorption features are detected in this configuration (see Supporting Information, SI), which confirms the excellent homogeneity of the fullerene layer.

In parallel polarization, the enhanced absorption bands are visible as sharp features on the broad plasmonic resonance. The top section of Figure 2 shows the SEIRA spectra of C_{60}. The

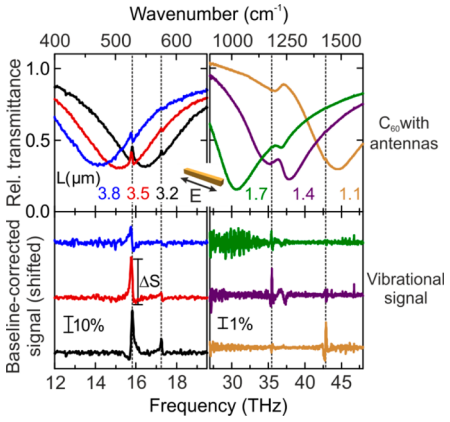

Figure 2. Relative transmittance of antennas covered with a 30 nm layer of C_{60} with varying lengths L (as given in the figure) resonant in the far- and mid-infrared (top). The corresponding baseline-corrected spectra feature typical asymmetric Fano-profiles originating from resonant interaction with the antennas (bottom). The inset indicates the polarization of the incident electric field. The fingerprint contrast ΔS gives the signal strength of the enhanced vibrational bands. Dashed vertical lines mark the spectral positions of the strongest molecular absorption features of C_{60}. Please note the different scales in the bottom panels.

vibrational bands of interest are located at 1428 and 1183 cm^{-1} in the case of the MIR region (left panels) and 577 and 527 cm^{-1} for the FIR region (right panels). In Figure 3, the respective spectra for measurements with C_{70} are depicted. Due to its reduced symmetry,[39] C_{70} exhibits more vibrational transitions than C_{60}. However, in the spectral region of interest, only one additional band can be found. This band, located at 458 cm^{-1} and the band at 1183 cm^{-1} are neglected in the data analysis, because of their low signal strength. To obtain a good signal-to-noise ratio on reasonable time scales, only the two strongest bands in the FIR (left panels) located at 577 and 534 cm^{-1} as well as the single band at 1428 cm^{-1} in the MIR (right panels) were regarded in the analysis of the SEIRA scaling.

The amino acid threonine was dissolved in methanol and spin-coated onto the antenna substrate to obtain a thin layer (see Methods). Threonine measurements were performed in parallel and perpendicular polarization with a bare Si substrate as reference.

Inspecting Figure 4, a total of five threonine absorption bands (marked by the dashed lines) can be detected. Absorption bands at 9.4 (314 cm^{-1}) and 6.8 THz (228 cm^{-1}) belong to $CC^{\alpha}N$ deformations and COO^{-} vibrations, respectively, while lower frequency absorption bands (5.6 (187 cm^{-1}), 4.95 (165 cm^{-1}), and 4.5 THz (150 cm^{-1})) can be assigned to hydrogen bond modes.[40] In perpendicular polarization, where no plasmonic enhancement is present, even the

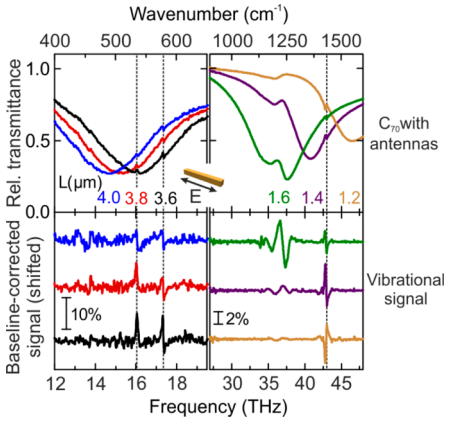

Figure 3. Relative transmittance (normally incident electric field polarized parallel to the antennas, as indicated by the inset) of antennas covered with C_{70} (30 nm) resonant in the far- and mid-infrared (top) and corresponding baseline-corrected spectra (bottom). Antenna lengths are given in the figure. Dashed lines mark the spectral positions of the strongest molecular absorption features of C_{70}. In comparison to C_{60} (see Figure 2), the vibrational band at 35.5 THz (1183 cm^{-1}) is much less pronounced and will therefore be neglected. Please note the different scales in the bottom panels.

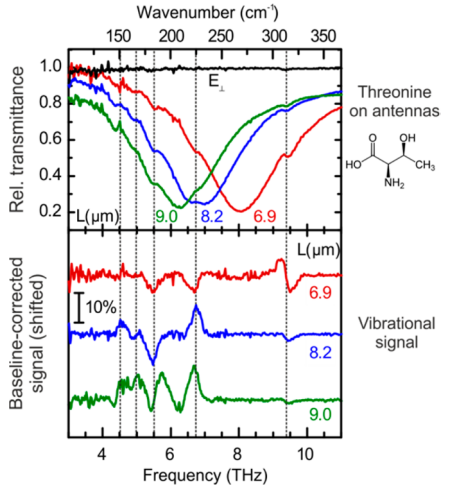

Figure 4. Relative transmittance measured in polarization parallel to the long antenna axis for a layer of the amino acid threonine of thickness of about 35 nm on antennas of varying length (green, blue, and red curves) and exemplary antenna spectrum measured in polarization perpendicular to the long antenna axis (black curve). Antenna lengths are given in the figure. The perpendicularly polarized spectrum was obtained on the L = 8.2 μm antenna field. (top) Corresponding baseline-corrected spectra. (bottom) The strongest vibrational absorption features of threonine are marked by dashed lines. The structural formula of threonine is indicated as well.

strongest absorption band located at 314 cm^{-1} is barely visible and the signal-to-noise ratio is extremely low. Vibrational bands located at lower frequencies can only be detected with SEIRA enhancement. In order to quantitatively evaluate the SEIRA enhancement, one has to obtain the signal strength of the enhanced vibrations. To exclude any possible influence from inhomogeneities of the threonine layer, threonine spectra in parallel polarization were normalized to the respective antenna spectra in perpendicular polarization. We then extract the enhanced absorption bands from the antenna resonances by performing a baseline approximation of the recorded spectra

DOI: 10.1021/acsphotonics.6b00534
ACS Photonics 2017, 4, 45−51

using the approach of asymmetric least-squares smoothing (AsLSS).[41] During this process, the spectral regions around the molecular absorption bands are excluded from the calculation of the baseline. The baseline-corrected transmittance, shown in Figures 2–4 (bottom panels) for C_{60}, C_{70}, and threonine, respectively, is obtained by calculating the ratio between measured spectra and approximated baseline. The vibrational signals exhibit a typical asymmetrical Fano line shape,[42] which is a signature of the resonant coupling between the broad antenna resonance and the narrow molecular absorption feature.[43] The absorption feature of the SiO_2 layer located at 1250 cm^{-1} is not excluded from the approximated baseline and is therefore only weakly visible in the baseline-corrected spectra. The signal strength ΔS is extracted from the baseline-corrected spectra by taking the peak-to-peak value of these vibrational signals (see Figure 2, bottom left panel). By normalizing them to the nonenhanced signals (see Figure 1c and Figure S2 in the SI) of the mere molecular film, we obtain the signal enhancement (for more details on the normalization, see SI).

The signal enhancement is then normalized to one antenna to account for the different antenna densities between varying arrays. This is achieved by multiplying the signal enhancement with the area that can be attributed to one antenna in an array given by $A_0 = (d_y + w)(d_x + L)$. The obtained quantity that we will refer to as signal enhancement per antenna therefore has μm^2 as units.

Inspecting the bottom panels of Figure 2–4, one can clearly identify a dependence of the enhanced vibrational signal strength on the antenna resonance position. Vibrational bands at spectral positions ω_{vib} closer to the antenna resonance frequency ω_{res} exhibit stronger enhancement. This is due to the fact that the near field of the antenna is strongest close to its far field resonance.[27,44,45] The influence of the tuning factor $\omega_{vib}/\omega_{res}$ on SEIRA has been studied in detail by Vogt et al.[46] They found that the SEIRA enhancement can be approximated by a Lorentzian, peaking at a tuning ratio $\omega_{vib}/\omega_{res} = 0.95$. To account for this, we apply an additional normalization by scaling up all values to this optimal tuning ratio. The resulting values are referred to as normalized signal enhancement per antenna.

Figure 4 reports on the strong dependence of this normalized signal enhancement per antenna on the vibrational frequency of the molecular absorption. The signal enhancement increases by 2 orders of magnitude when tuning from vibrations located in the MIR range (1428 and 1183 cm^{-1}) to vibrations located in the single digit THz range (314 and 228 cm^{-1}). This can be attributed to mainly two effects. On the one hand, antennas resonant at lower frequencies are longer (in our case, approximately by a factor of 4) and therefore offer a larger surface area with significant near fields. However, this trivial effect can only partially explain our results, as the near field of a resonantly excited rod antenna is mostly concentrated around the antenna tips.[47,48] We affirm this notion by determining the near field distribution of antennas of different resonance frequencies by means of finite-difference time-domain (FDTD) simulations (see SI for details). In the simulations, 50% of the total integrated electric near field intensity was confined in a volume of about 2 × 5% of the full antenna length located around the tips (see Figure S3 in the SI). Thus, the additional number of molecules attached to the surface of a larger antenna is exposed to relatively weak electric fields only.

Therefore, a more significant effect must influence the enhancement. We propose that this effect stems from an increased dipole moment expected for longer antennas. Consequently, these antennas exhibit higher near field intensities and thus a larger signal enhancement (SE). This is due to the fact that the SE in SEIRA is known to be directly proportional to the intensity of the plasmonic near field[49] $SE \propto I \propto |E|^2$. In order to confirm this assumption, the near field intensity $|E|^2$ obtained from FDTD simulations is integrated over the volume of a 30 nm thick shell around the antenna, corresponding to the volume where the molecules are located in the experiment. By performing this integration, we take both the extent as well as the magnitude of the near field into account. We thus acquire an integrated near field intensity that is expected to exhibit the same scaling behavior as the SEIRA enhancement.

Furthermore, we conclude from classical antenna theory that the integrated near field intensity around an antenna resonantly excited at a wavelength λ is proportional to the cube of the wavelength.[50,51]

$$SE \propto I \propto \lambda^3 \tag{1}$$

Even though certain adaptations have to be made for plasmonic antennas at optical frequencies when compared to the macroscopic case,[48,52,53] this correlation still holds true.

To verify the scaling behavior, we normalize eq 1 by a constant factor to match the absolute values to the experimentally measured and numerically calculated ones. The results in Figure 5 indicate excellent agreement between

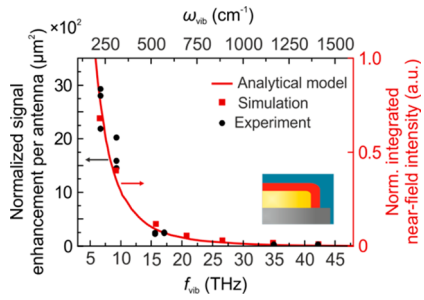

Figure 5. Experimentally determined signal enhancement (enhanced vibrational signal ΔS divided by the not-enhanced vibrational strength), for different vibrational frequencies f_{vib} (black dots). The signal enhancement is normalized to the antenna density and therefore has μm^2 as unit. The normalized integrated near-field intensity (red squares) is calculated from FDTD simulations by integrating over a 30 nm shell around the antenna. The inset depicts a schematic drawing of the simulated structure and the volume of integration (red area). The red line shows the normalized integrated near-field intensities obtained from classical antenna theory. Both, simulation and analytical calculations show a good qualitative agreement with the experimental results.

experiment, simulation, and analytical calculation. The SEIRA enhancement as well as the integrated near field intensity increases with decreasing resonance frequency (and therefore increasing length) of the nanoantenna. From classical antenna theory, we obtained a proportionality to λ^3 (see eq 1) caused by two effects. First, the molecular volume and therefore the applied integral grows with the antenna length. This corresponds to the first power of λ in eq 1. The factor λ^2 originates from the increase of the near field intensity, which is proportional to the squared current amplitude. Such behavior is

DOI: 10.1021/acsphotonics.6b00534
ACS Photonics 2017, 4, 45–51

found in literature when comparing near field enhancements of nanoantennas resonant at different spectral regions.[17,27,28,54] It can be understood in terms of an increased dipole moment created when a plasmon is resonantly excited in a larger antenna.

The excellent agreement of the scaling behavior also indicates that the influence of the collective excitation in periodic antenna arrays on SEIRA does not significantly depend on the selected frequency. As mentioned before, the geometry of the antenna arrays was designed in a way to benefit from the additional SEIRA enhancement that takes place close to the collective excitation. Classical antenna theory, as applied here however is only valid for a single antenna and does not include any coupling mechanisms. Therefore, the effect of the collective mode on SEIRA must depend only weakly on the resonance frequency. That way, it only boosts the signal enhancement at all frequencies, without significantly influencing the scaling.

Finally, we estimate the maximum SEIRA enhancement factors obtained from our experiments. In order to compare our values to previous work, we use the approach suggested by D'Andrea et al.[47] and assign $2 \times w \times h$ as the area that contributes to the SEIRA signal of an antenna. It is noteworthy, though, that this is only a rough approximation (see Figure S2 in the SI). We thus obtain the enhancement factor by dividing the signal enhancement per antenna by $2 \times w \times h$. We achieve enhancement factors of 1200 for the MIR spectral region and 128000 for the single digit THz spectral region in the case of the best tuning. Compared to similar studies conducted in the MIR spectral region,[34,35,46,55] the enhancement factor obtained here is about 1 order of magnitude smaller. However, this is expected, as we use float-zone Si as a substrate, which has the advantage to remain transparent down to the gigahertz regime,[56] but due to its high refractive index suppresses the SEIRA enhancement.[57]

CONCLUSION

We demonstrated the resonant antenna-enhanced spectroscopy of molecules over the spectral range of the molecular fingerprint region from 4.5 to 45 THz (6.7−67 μm wavelength, 150−1500 cm^{-1}) using standard FTIR spectroscopy. In our experiments, we observed an increase of the SEIRA enhancement of 2 orders of magnitude at lower frequencies. The scaling behavior of the SEIRA enhancement was in excellent agreement with the integrated near field intensities of the corresponding resonantly excited nanoantennas, obtained from both numerical FDTD simulation as well as classical antenna theory. It was demonstrated that the SEIRA enhancement exhibits a proportionality to λ^3 in a frequency range of 1 order of magnitude. This is particularly promising as THz spectroscopy suffers substantially more from small absorption cross sections of molecules than IR spectroscopy due to the massive mismatch of the dimensions between molecule and wavelength of the THz radiation.

METHODS

Sample Fabrication. The antenna arrays were fabricated on float-zone silicon via standard electron-beam lithography (Raith eLINE) in double layer poly(methyl methacrylate) resist (200 and 950 K, Allresist). One surface of the wafer was angled by 1° to avoid the formation of Fabry−Perot resonances. After development, a 5 nm Cr adhesion and a 95 nm Au layer was thermally evaporated followed by a lift-off procedure in an *N*-ethyl-2-pyrrolidon (NEP) based remover (Allresist). The final antenna array size was 200×200 μm^2 respectively 1×1 mm^2.

C_{60}/C_{70} Evaporation. C_{60} and C_{70} thin films are deposited via vacuum sublimation at a pressure of $<10^{-7}$ mbar. For both materials, same deposition rates (±20%) of 1 nm·min^{-1} are used. For this, the temperature of the evaporation crucible is elevated to about 450 °C (520 °C) for the evaporation of C_{60} (C_{70}). Thin films of both materials exhibit excellent homogeneity. The relative transmittance of bare 30 nm thick layers of C_{60} and C_{70} are shown in Figure 1c.

Spin-Coating of Threonine. L-Threonine (≥98%, Sigma-Aldrich) was dissolved in methanol until saturation concentration was reached. The threonine solution was then spin-coated onto antenna substrates for 180 s at 700 rpm, followed by 40 s at 3000 rpm. Prior to the spin-coating procedure, antenna substrates were cleaned for 5 min in oxygen plasma. The thickness of the threonine layer can be estimated to be about 35 nm, as obtained from tactile surface profilometry (Veeco Dektak 150).

IR Transmittance Measurements. Relative transmittance measurements in the spectral region from 900 to 1600 cm^{-1} were performed using a Bruker Hyperion 2000 IR microscope with a liquid nitrogen-cooled mercury cadmium telluride (MCT) detector using a square aperture of the size 100×100 μm^2. For the detection of the FIR signal (150−650 cm^{-1}), an identically constructed microscope equipped with a liquid helium-cooled bolometer as a detector was used. For the FIR measurements of C_{70} the aperture size was 200×200 μm^2, while for the threonine measurements it was 1×1 mm^2.

Scanning Electron Micrographs. The scanning electron micrograph was acquired with an S-4800 scanning electron microscope (Hitachi Company).

FDTD Simulations. Near field distributions were calculated using the commercial FDTD software Lumerical FDTD-Solutions v8.5.3. Details on the simulation setup are found in ref 58.

ASSOCIATED CONTENT

Supporting Information

The Supporting Information is available free of charge on the ACS Publications website at DOI: 10.1021/acsphotonics.6b00534.

Relative transmittance spectra of antenna arrays in parallel and perpendicular polarization with C_{60} and C_{70} layers, relative transmittance measurements of threonine layers on antenna arrays in perpendiculat polarization and of a reference layer on bare Si, integrated near field intensities for varying integration volumes around antenna tips (PDF).

AUTHOR INFORMATION

Corresponding Author

*E-mail: f.neubrech@pi4.uni-stuttgart.de.

ORCID

Ksenia Weber: 0000-0002-9836-8457

Author Contributions

The manuscript was written through contributions of all authors. All authors have given approval to the final version of the manuscript.

Notes

The authors declare no competing financial interest.

DOI: 10.1021/acsphotonics.6b00534
ACS Photonics 2017, 4, 45−51

■ ACKNOWLEDGMENTS

The authors gratefully acknowledge financial support by the ERC Advanced Grant COMPLEXPLAS, DFG, Baden-Württemberg Stiftung, VW Stiftung, Alexander-von-Humboldt Stiftung, BMBF, and the Heidelberg Graduate School of Fundamental Physics.

■ REFERENCES

(1) Jepsen, P. U.; Cooke, D. G.; Koch, M. Terahertz Spectroscopy and Imaging – Modern Techniques and Applications. *Laser Photon. Rev.* **2012**, *6*, 124–166.
(2) Feuillet-Palma, C.; Todorov, Y.; Vasanelli, A.; Sirtori, C. Strong near Field Enhancement in THz Nano-Antenna Arrays. *Sci. Rep.* **2013**, *3*, 1361.
(3) Gallot, G.; Jamison, S. P.; McGowan, R. W.; Grischkowsky, D. Terahertz Waveguides. *J. Opt. Soc. Am. B* **2000**, *17*, 851–863.
(4) Huber, A. J.; Keilmann, F.; Wittborn, J.; Aizpurua, J.; Hillenbrand, R. Terahertz Near-Field Nanoscopy of Mobile Carriers in Single Semiconductor Nanodevices. *Nano Lett.* **2008**, *8*, 3766–3770.
(5) Lim, M.; Choi, S.-J.; Lee, G.-S.; Seol, M.-L.; Do, Y.; Choi, Y.-K.; Han, H. Terahertz Time-Domain Spectroscopy of Anisotropic Complex Conductivity Tensors in Silicon Nanowire Films. *Appl. Phys. Lett.* **2012**, *100*, 211102.
(6) Shi, W.; Ding, Y. J. A Monochromatic and High-Power Terahertz Source Tunable in the Ranges of 2.7–38.4 and 58.2–3540 Mm for Variety of Potential Applications. *Appl. Phys. Lett.* **2004**, *84*, 1635–1637.
(7) Bardhan, R.; Grady, N. K.; Cole, J. R.; Joshi, A.; Halas, N. J. Fluorescence Enhancement by Au Nanostructures: Nanoshells and Nanorods. *ACS Nano* **2009**, *3*, 744–752.
(8) Kinkhabwala, A.; Yu, Z.; Fan, S.; Avlasevich, Y.; Mullen, K.; Moerner, W. E. Large Single-Molecule Fluorescence Enhancements Produced by a Bowtie Nanoantenna. *Nat. Photonics* **2009**, *3*, 654–657.
(9) Nie, S.; Emory, S. R. Probing Single Molecules and Single Nanoparticles by Surface-Enhanced Raman Scattering. *Science* **1997**, *275*, 1102–1106.
(10) Fazio, B.; D'Andrea, C.; Bonaccorso, F.; Irrera, A.; Calogero, G.; Vasi, C.; Gucciardi, P. G.; Allegrini, M.; Toma, A.; Chiappe, D.; Martella, C.; de Mongeot, F. B. Re-Radiation Enhancement in Polarized Surface-Enhanced Resonant Raman Scattering of Randomly Oriented Molecules on Self-Organized Gold Nanowires. *ACS Nano* **2011**, *5*, 5945–5956.
(11) Neubrech, F.; Aizpurua, J.; Lopes, M.; de la Chapelle, M. L.; Pucci, A. Plasmon-Resonance Enhanced Infrared Spectroscopy Using Gold Nanoantennas Fabricated by Electron-Beam Lithography. In *Frontiers in Optics 2008/Laser Science XXIV/Plasmonics and Metamaterials/Optical Fabrication and Testing*; Optical Society of America, 2008; p MThD5.
(12) Osawa, M.; Ataka, K.-I.; Yoshii, K.; Nishikawa, Y. Surface-Enhanced Infrared Spectroscopy: The Origin of the Absorption Enhancement and Band Selection Rule in the Infrared Spectra of Molecules Adsorbed on Fine Metal Particles. *Appl. Spectrosc.* **1993**, *47*, 1497–1502.
(13) Hartstein, A.; Kirtley, J. R.; Tsang, J. C. Enhancement of the Infrared Absorption from Molecular Monolayers with Thin Metal Overlayers. *Phys. Rev. Lett.* **1980**, *45*, 201–204.
(14) Neuman, T.; Huck, C.; Vogt, J.; Neubrech, F.; Hillenbrand, R.; Aizpurua, J.; Pucci, A. Importance of Plasmonic Scattering for an Optimal Enhancement of Vibrational Absorption in SEIRA with Linear Metallic Antennas. *J. Phys. Chem. C* **2015**, *119*, 26652–26662.
(15) Rodrigo, D.; Limaj, O.; Janner, D.; Etezadi, D.; Garcia de Abajo, F. J.; Pruneri, V.; Altug, H. Mid-Infrared Plasmonic Biosensing with Graphene. *Science* **2015**, *349*, 165–168.
(16) Wang, T.; Nguyen, V. H.; Buchenauer, A.; Schnakenberg, U.; Taubner, T. Surface Enhanced Infrared Spectroscopy with Gold Strip Gratings. *Opt. Express* **2013**, *21*, 9005–9010.
(17) Neubrech, F.; Pucci, A.; Cornelius, T. W.; Karim, S.; Garcia-Etxarri, A.; Aizpurua, J. Resonant Plasmonic and Vibrational Coupling in a Tailored Nanoantenna for Infrared Detection. *Phys. Rev. Lett.* **2008**, *101*, 157403.
(18) Weis, P.; Garcia-Pomar, J. L.; Beigang, R.; Rahm, M. Hybridization Induced Transparency in Composites of Metamaterials and Atomic Media. *Opt. Express* **2011**, *19*, 23573–23580.
(19) Park, H.-R.; Ahn, K. J.; Han, S.; Bahk, Y.-M.; Park, N.; Kim, D.-S. Colossal Absorption of Molecules Inside Single Terahertz Nanoantennas. *Nano Lett.* **2013**, *13*, 1782–1786.
(20) Berrier, A.; Albella, P.; Poyli, M. A.; Ulbricht, R.; Bonn, M.; Aizpurua, J.; Rivas, J. G. Detection of Deep-Subwavelength Dielectric Layers at Terahertz Frequencies Using Semiconductor Plasmonic Resonators. *Opt. Express* **2012**, *20*, 5052–5060.
(21) Berrier, A.; Schaafsma, M. C.; Nonglaton, G.; Bergquist, J.; Rivas, J. G. Selective Detection of Bacterial Layers with Terahertz Plasmonic Antennas. *Biomed. Opt. Express* **2012**, *3*, 2937–2949.
(22) Ramer, J.-M.; Ospald, F.; von Freymann, G.; Beigang, R. Generation and Detection of THz Radiation up to 4.5 THz Using LTG-GaAs PCAs Illuminated at 1560 Nm. In *2013 38th International Conference on Infrared, Millimeter, and Terahertz Waves (IRMMW-THz)*; IEEE, 2013.
(23) Ramer, J. M.; Von Freymann, G. A Terahertz Time-Domain Spectroscopy-Based Network Analyzer. *J. Lightwave Technol.* **2015**, *33*, 403–407.
(24) Taday, P. F.; Bradley, I. V.; Arnone, D. D.; Pepper, M. Using Terahertz Pulse Spectroscopy to Study the Crystalline Structure of a Drug: A Case Study of the Polymorphs of Ranitidine Hydrochloride. *J. Pharm. Sci.* **2003**, *92*, 831–838.
(25) Toma, A.; Tuccio, S.; Prato, M.; Donato, F. De; Perucchi, A.; Pietro, P. Di; Marras, S.; Liberale, C.; Zaccaria, R. P.; Angelis, F. De; Manna, L.; Lupi, S.; Fabrizio, E. Di; Razzari, L. Squeezing Terahertz Light into Nanovolumes: Nanoantenna Enhanced Terahertz Spectroscopy (NETS) of Semiconductor Quantum Dots. *Nano Lett.* **2015**, *15*, 386–391.
(26) Bukasov, R.; Ali, T. A.; Nordlander, P.; Shumaker-Parry, J. S. Probing the Plasmonic Near-Field of Gold Nanocrescent Antennas. *ACS Nano* **2010**, *4*, 6639–6650.
(27) Alonso-González, P.; Albella, P.; Neubrech, F.; Huck, C.; Chen, J.; Golmar, F.; Casanova, F.; Hueso, L. E.; Pucci, A.; Aizpurua, J.; Hillenbrand, R. Experimental Verification of the Spectral Shift between near- and Far-Field Peak Intensities of Plasmonic Infrared Nanoantennas. *Phys. Rev. Lett.* **2013**, *110*, 1–6.
(28) Sandu, T. Near-Field and Extinction Spectra of Rod-Shaped Nanoantenna Dimers. *Proc. Romanian Acad., Ser. A* **2014**, *15*, 338–345.
(29) Neuman, T.; Alonso-González, P.; Garcia-Etxarri, A.; Schnell, M.; Hillenbrand, R.; Aizpurua, J. Mapping the near Fields of Plasmonic Nanoantennas by Scattering-Type Scanning near-Field Optical Microscopy. *Laser Photonics Rev.* **2015**, *9*, 637–649.
(30) Maier, S. A. *Plasmonics: Fundamentals and Applications*; Springer Science & Business Media, 2007.
(31) Meilunas, R.; Chang, R. P. H.; Liu, S.; Jensen, M.; Kappes, M. M. Infrared and Raman Spectra of C_{60} and C_{70} Solid Films at Room Temperature. *J. Appl. Phys.* **1991**, *70*, 5128.
(32) Abb, M.; Wang, Y.; Papasimakis, N.; de Groot, C. H.; Muskens, O. L. Surface-Enhanced Infrared Spectroscopy Using Metal Oxide Plasmonic Antenna Arrays. *Nano Lett.* **2014**, *14*, 346–352.
(33) Weber, D.; Albella, P.; Alonso-González, P.; Neubrech, F.; Gui, H.; Nagao, T.; Hillenbrand, R.; Aizpurua, J.; Pucci, A. Longitudinal and Transverse Coupling in Infrared Gold Nanoantenna Arrays: Long Range versus Short Range Interaction Regimes. *Opt. Express* **2011**, *19*, 15047–15061.
(34) Adato, R.; Yanik, A. A.; Amsden, J. J.; Kaplan, D. L.; Omenetto, F. G.; Hong, M. K.; Erramilli, S.; Altug, H. Ultra-Sensitive Vibrational Spectroscopy of Protein Monolayers with Plasmonic Nanoantenna Arrays. *Proc. Natl. Acad. Sci. U. S. A.* **2009**, *106*, 19227–19232.
(35) Bagheri, S.; Weber, K.; Gissibl, T.; Weiss, T.; Neubrech, F.; Giessen, H. Fabrication of Square-Centimeter Plasmonic Nanoantenna Arrays by Femtosecond Direct Laser Writing Lithography: Effects of

DOI: 10.1021/acsphotonics.6b00534
ACS Photonics 2017, 4, 45–51

Collective Excitations on SEIRA Enhancement. *ACS Photonics* **2015**, *2*, 779−786.
(36) Adato, R.; Yanik, A. A.; Wu, C.-H.; Shvets, G.; Altug, H. Radiative Engineering of Plasmon Lifetimes in Embedded Nanoantenna Arrays. *Opt. Express* **2010**, *18*, 4526−4537.
(37) Maß, T. W. W.; Taubner, T. Incident Angle-Tuning of Infrared Antenna Array Resonances for Molecular Sensing. *ACS Photonics* **2015**, *2*, 1498−1504.
(38) Neubrech, F.; Weber, D.; Enders, D.; Nagao, T.; Pucci, A. Antenna Sensing of Surface Phonon Polaritons. *J. Phys. Chem. C* **2010**, *114*, 7299−7301.
(39) Refson, K.; Parker, S. F. Assignment of the Internal Vibrational Modes of C_{70} by Inelastic Neutron Scattering Spectroscopy and Periodic-DFT. *ChemistryOpen* **2015**, *4*, 620−625.
(40) Matei, A.; Drichko, N.; Gompf, B.; Dressel, M. Far-Infrared Spectra of Amino Acids. *Chem. Phys.* **2005**, *316*, 61−71.
(41) Eilers, P. H. C. A Perfect Smoother. *Anal. Chem.* **2003**, *75*, 3631−3636.
(42) Fano, U. Effects of Configuration Interaction on Intensities and Phase Shifts. *Phys. Rev.* **1961**, *124*, 1866−1878.
(43) Giannini, V.; Francescato, Y.; Amrania, H.; Phillips, C. C.; Maier, S. A. Fano Resonances in Nanoscale Plasmonic Systems: A Parameter-Free Modeling Approach. *Nano Lett.* **2011**, *11*, 2835−2840.
(44) Zuloaga, J.; Nordlander, P. On the Energy Shift between Near-Field and Far-Field Peak Intensities in Localized Plasmon Systems. *Nano Lett.* **2011**, *11*, 1280−1283.
(45) Kats, M. A.; Yu, N.; Genevet, P.; Gaburro, Z.; Capasso, F. Effect of Radiation Damping on the Spectral Response of Plasmonic Components. *Opt. Express* **2011**, *19*, 21748−21753.
(46) Vogt, J.; Huck, C.; Neubrech, F.; Toma, A.; Gerbert, D.; Pucci, A. Impact of the Plasmonic Near- and Far-Field Resonance-Energy Shift on the Enhancement of Infrared Vibrational Signals. *Phys. Chem. Chem. Phys.* **2015**, *17*, 21169−21175.
(47) D'Andrea, C.; Bochterle, J.; Toma, A.; Huck, C.; Neubrech, F.; Messina, E.; Fazio, B.; Marag, O. M.; Di Fabrizio, E.; Lamy; de La Chapelle, M.; Gucciardi, P. G.; Pucci, A. Optical Nanoantennas for Multiband Surface-Enhanced Infrared and Raman Spectroscopy. *ACS Nano* **2013**, *7*, 3522−3531.
(48) Taminiau, T. H.; Moerland, R. J.; Segerink, F. B.; Kuipers, L.; van Hulst, N. F. Lambda/4 Resonance of an Optical Monopole Antenna Probed by Single Molecule Fluorescence. *Nano Lett.* **2007**, *7*, 28−33.
(49) Dregely, D.; Neubrech, F.; Duan, H.; Vogelgesang, R.; Giessen, H. Vibrational near-Field Mapping of Planar and Buried Three-Dimensional Plasmonic Nanostructures. *Nat. Commun.* **2013**, *4*, 2237.
(50) Balanis, C. A. *Antenna Theory: Analysis and Design*; John Wiley & Sons, 2016.
(51) Orfanidis, S. J. *Electromagnetic Waves and Antennas*; Prentice Hall, 2003.
(52) Dorfmüller, J.; Vogelgesang, R.; Khunsin, W.; Rockstuhl, C.; Etrich, C.; Kern, K. Plasmonic Nanowire Antennas: Experiment, Simulation, and Theory. *Nano Lett.* **2010**, *10*, 3596−3603.
(53) Novotny, L.; van Hulst, N. Antennas for Light. *Nat. Photonics* **2011**, *5*, 83−90.
(54) Sandu, T.; Buiculescu, V. Near-Field Enhancement of a Rod-like Nanoantenna: Elctrostatic versus Fully Retarded Results. In *CAS 2012 (International Semiconductor Conference)*; 2012; Vol. *2*, pp 415−418.
(55) Bagheri, S.; Giessen, H.; Neubrech, F. Large-Area Antenna-Assisted SEIRA Substrates by Laser Interference Lithography. *Adv. Opt. Mater.* **2014**, *2*, 1050−1056.
(56) Dai, J.; Zhang, J.; Zhang, W.; Grischkowsky, D. Terahertz Time-Domain Spectroscopy Characterization of the Far-Infrared Absorption and Index of Refraction of High-Resistivity, Float-Zone Silicon. *J. Opt. Soc. Am. B* **2004**, *21*, 1379−1386.
(57) Teschner, U.; Hübner, K. IR-Spectroscopic Data of Thin Insulating Films on Semiconductors. New Methods of Interpretation and Analysis. *Phys. Status Solidi B* **1990**, *159*, 917−926.
(58) Neubrech, F.; Beck, S.; Glaser, T.; Hentschel, M.; Giessen, H.; Pucci, A. Spatial Extent of Plasmonic Enhancement of Vibrational Signals in the Infrared. *ACS Nano* **2014**, *8*, 6250−6258.

DOI: 10.1021/acsphotonics.6b00534
ACS Photonics 2017, 4, 45−51